LASER & PHOTONICS REVIEWS

www.lpr-journal.org

100-Layer Error-Free 5D Optical Data Storage by Ultrafast Laser Nanostructuring in Glass

Huijun Wang, Yuhao Lei, Lei Wang, Masaaki Sakakura, Yanhao Yu, Gholamreza Shayeganrad, and Peter G. Kazansky*

The demand for energy efficient data storage technologies with high capacity and long life span is increasingly growing due to the explosion of digital information in modern society. Here, a 5D optical data storage with high capacity and ultralong lifetime is realized by femtosecond-laser-induced anisotropic nanopore structures (type *X* modification) in silica glass. The ultrahigh transmission of this birefringent modification, >99% in the visible range, allows recording and retrieving thousands of layers of multibit digital data practically. Type *X* formation is associated with moderate free carrier density produced close to the energy threshold of avalanche ionization. Higher retardance with increased repetition rate at low pulse energy is attributed to accumulation of defects (nonbridging oxygen hole centers), enabling rapid imprinting of voxels by megahertz-rate pulses. Data recording of 7 bits per voxel, i.e., 2^5 azimuth angles and 2^2 retardance levels is experimentally demonstrated with readout error as small as 0.6%. Furthermore, "The Hitchhiker's Guide to the Galaxy" by Douglas Adams is optically recorded with a data writing speed of 8 kB s^{-1} in 100 layers of voxels and the proven data readout accuracy of 100%.

1. Introduction

To cope with the ever-increasing storage demand, a wide range of data storage techniques have been developed, among which the magnetization-based storages like hard disk drivers (HDDs) and magnetic tapes account for a large proportion, but HDDs fall short of capacity, energy efficiency, and lifetime, while the weakness of magnetic tapes is longer access latency and degradation. On the other hand, optical data storage is also an attractive technique due to low energy consumption, nonvolatile property, and unchangeable stored data by a hacker, making it a potential candidate for data archiving and internet backup. However, conventional optical storage techniques based on planar technology such as compact discs (CDs) and digital video discs (DVDs) have a maximum capacity of tens of gigabytes per disk and can only be preserved up to a decade.[1–3] Therefore, a new storage method with the merits of both high capacity and long life span is desired.

In recent years, ultrafast laser direct writing,[4–6] in particular nanostructuring, in transparent materials has been widely studied because of its unique advantages such as rapid deposition of energy with high precision. Compared with longer laser pulses (larger than a few picoseconds), femtosecond laser pulses can produce modifications inside the material without collateral damage in nonthermal regime,[7,8] suggesting that femtosecond laser is the most promising tool for 3D optical data storage.[9,10] Normally, only one bit of information can be stored in a data voxel, whereas, more bits can be recorded by multiplex technology, resulting in a larger storage capacity and a higher writing/readout speed, which is an alternative to holographic data storage.[11,12] Additional dimensions have been implemented by several parameters such as intensity, polarization, and wavelength.[13–16] More recently, based on self-assembled nanogratings (type 2 modification)[17–20] produced by ultrafast laser writing in silica glass, recording and retrieval of multiplexed digital data were demonstrated.[21,22] Three spatial dimensions and two optical ones (the slow axis orientation and the retardance) were exploited to realize 5D data storage. In addition to the benefits of multiplexing, the 5D optical data storage utilizing rewriteable[23–25] nanogratings in fused silica has high chemical and thermal stability and high optical damage threshold,[26] generating seemingly unlimited lifetime at room temperature.

Despite the aforementioned favorable features of nanograting-based 5D optical data storage, the low transmission in the visible range, originated from the scattering loss,[27] limits the accurate readout of multilayer data storage. Recently, a new type of ultrafast-laser-induced modification in silica glass, which consists of randomly distributed nanopores elongated in the direction perpendicular to the polarization direction of the writing laser beam (type *X*), has been demonstrated, providing

H. Wang, Y. Lei, L. Wang, M. Sakakura, Y. Yu, G. Shayeganrad, P. G. Kazansky
Optoelectronics Research Centre
University of Southampton
Southampton SO17 1BJ, UK
E-mail: Huijun.Wang@soton.ac.uk

The ORCID identification number(s) for the author(s) of this article can be found under https://doi.org/10.1002/lpor.202100563

DOI: 10.1002/lpor.202100563

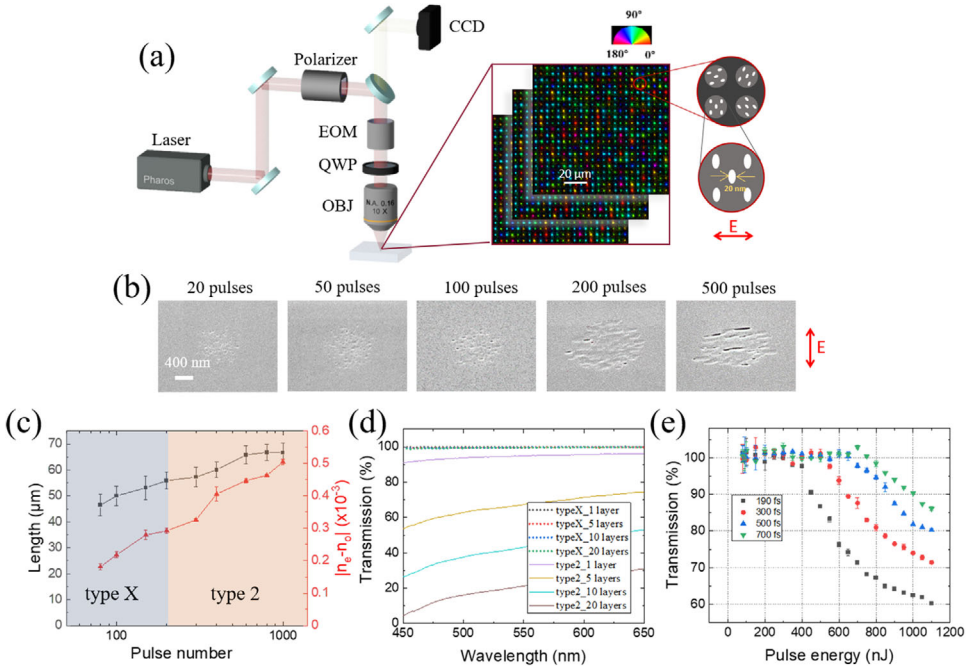

Figure 1. Femtosecond laser writing inside silica glass. a) Schematic diagram of the experimental setup utilized in femtosecond laser writing and 5D optical data storage. EOM: electro-optic modulator, QWP: quarter waveplate, OBJ: objective, CCD: charge coupled device, E: electric field of the incident light. b) SEM images of type *X* and type 2 modifications after polishing and etching with a lens NA = 0.16 and laser pulse energy, repetition rate, and duration of 690 nJ, 500 kHz, and 300 fs, respectively, for different laser pulse numbers. c) The measured longitudinal length (black square) and calculated birefringence (red triangle) of the birefringent nanostructures versus pulse number. The dots in blue region correspond to type *X* modification, while that in orange region represent type 2. d) Transmittance of type *X* and type 2 birefringent voxels with 1, 5, 10, and 20 layers. e) Nonlinear transmission for single laser pulse versus pulse energy for different pulse durations focused by 0.16 NA lens.

controllable birefringent structures with transmittance as high as 99% in the visible range.[28]

Here, we demonstrated a multilayer ultralow-loss 5D data storage with 100% readout accuracy by investigating different processing parameters, including pulse duration, repetition rate, and focusing condition. We also realized experimentally record high 7 bits per voxel with ≈99% accuracy, contributing to pragmatic data storage with high capacity. As a demonstration, "The Hitchhiker's Guide to the Galaxy" by Douglas Adams was optically encrypted into 100 layers in silica glass with an increased data writing speed of 8 kB s^{-1} achieved by tighter focusing in combination with higher repetition rate, which was retrieved with accuracy of 100%.

2. Results and Discussion

2.1. Properties of Type *X* Modification

Data recording experiments were carried out with a mode-locked regenerative amplified femtosecond laser system operating at 1030 nm with variable repetition rate (R.R.) and pulse duration (τ) (**Figure 1**a). The scanning electron microscope (SEM) images of the low-loss birefringent modification were captured with different number of pulses (N_p) at R.R. of 500 kHz, pulse duration of 300 fs, pulse energy of 690 nJ, numerical aperture (NA) of 0.16, and scanning speed of 1 mm s^{-1} (Figure 1b). A number of randomly distributed and seemingly isotropic nanopores with diameter of ≈20 nm were observed in the photoexcited region at $N_p = 20$, indicating barely detectable birefringence. At $N_p = 50$, the nanopores were clearly elongated perpendicular to the polarization of the writing beam. As the pulse number increases, the density and aspect ratio of nanopores increase, which is consistent with the increase of the birefringence with the pulse number. The nanopores experienced a sharp change around $N_p = 200$ to the nanoplanes or self-assembled nanogratings (type 2). The length of the birefringent structure along the beam propagation direction increases with the number of pulses (Figure 1c). The birefringence, the difference between refractive indices for ordinary and extraordinary waves $|n_e - n_o|$, was calculated from measurements of retardance and the longitudinal length of the structure (Δn_b = Ret./l) and was found to be on the order of $\approx 10^{-4}$ for both type *X* and type 2 modifications. The birefringence of nanogratings and elongated-nanopore-based modifications originates from form birefringence of anisotropic nanostructures and localized-stress-induced birefringence.[29] However, the stress is negligible in type *X* modification, so its birefringence is mainly attributed to form birefringence of flattened nanopores. The transmittance of the ultralow-loss modification (type *X*) is higher than 99% in the visible (VIS) and the near infrared (NIR) spectral regions.[28] It is noticeable that the transmittance of 20-layer type *X* in the visible region (450–650 nm) is still as high as 99% (Figure 1d). By contrast, for type 2 modification, the transmittance is ≈90% at 550 nm for a single layer and it dramatically reduces to ≈20% for 20 layers of voxels, which restricts the data readout with high accuracy.

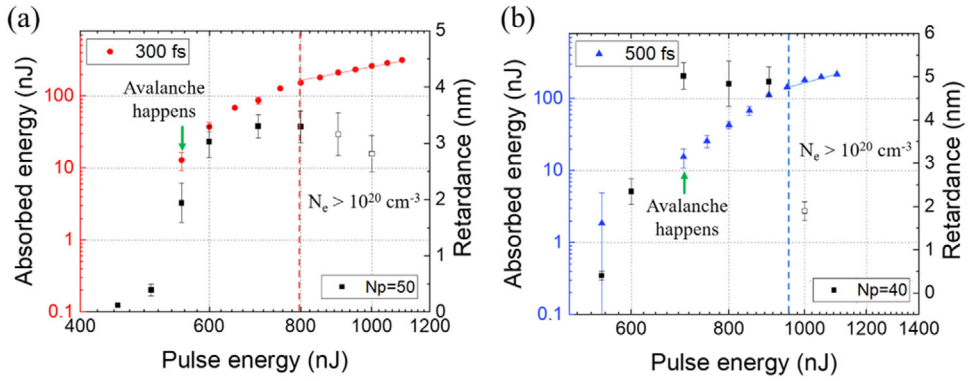

Figure 2. Absorbed energy of single laser pulse and retardance of birefringent voxels versus pulse energy for pulse durations of a) 300 fs and b) 500 fs. Each voxel is written by 50 (40) pulses with duration of 300 (500) fs focused by 0.16 NA lens. The solid and hollow black squares represent type *X* and type 2 modifications, respectively.

In order to investigate the influence of laser pulse duration on energy deposition, we measured the nonlinear transmission for single laser pulse as a function of pulse energy for different pulse durations of 190, 300, 500, and 700 fs at 1030 nm wavelength, focused by 0.16 NA lens (Figure 1e). The transmission drop from nearly 100% requires more pulse energy for a longer pulse duration,[30,31] e.g., 800 nJ for 700 fs and 350 nJ for 190 fs. For the shortest pulse duration (τ = 190 fs), isotropic index increase (type 1) was the most common modification at low pulse energy, but type *X* modification was produced in a narrow pulse energy range (around 1000 nJ) possibly due to the lack of self-trapped triplet excitons[28] (Figures S1 and S2, Supporting Information). By contrast, for pulse durations of 300 and 500 fs, both type *X* and type 2 were observed in a large pulse energy range from 450 to 1000 nJ. The absorbance of single laser pulse for type *X* modification was from about 2% to 25% depending on pulse energy and duration. For example, 15% pulse energy was absorbed for pulse duration of 300 fs and energy of 690 nJ.

The sharp drop in the transmission from 100% (Figure 1e) is the signature of avalanche ionization.[30] For 0.16 NA and pulse duration of 300 fs, the avalanche ionization happens at pulse energy of about 550 nJ (7.2 TW cm^{-2}) and dominates at 800 nJ (10.5 TW cm^{-2}) (**Figure 2**a). Type *X* modification was produced by 50 pulses for pulse energies between 550 and 800 nJ, while type 2 was observed above 800 nJ. This could indicate that moderate free electron concentration (N_e) of 10^{18}–10^{19} cm^{-3}[31,32] is responsible for elongated nanopore formation where the pulse energy is just above the threshold of avalanche ionization. The higher free carrier density of about 10^{20} cm^{-3}[33,34] with larger pulse energy is required for the formation of nanogratings (type 2). Similar pulse energy dependence of birefringent modifications was observed for 500 fs pulses (Figure 2b) and different pulse numbers (Figure S3, Supporting Information).

2.2. Demonstration of Data Recording in Silica Glass

First, we explored the critical parameters of type *X* formation for data storage application including laser repetition rate and NA of the aspheric lens. Pulse duration of 300 fs was chosen due to the wider parameter window for pulse number and pulse energy (Figures S1 and S2, Supporting Information). The pulse energy range for type *X* formation decreases with the increase of the effective numerical aperture, however, the intensity range for type *X*, from about 6 to 12 TW cm^{-2}, is almost the same for all NAs. The maximum retardance for type *X* modification is smaller with larger NA due to the shorter structure length. However, the required number of pulses for a birefringent voxel and the lateral size of the modification can be reduced with higher NA, resulting in faster data writing and higher data capacity. For pulse duration of 300 fs, the modification threshold 6 TW cm^{-2} in multipulse case is corresponding to fluence of 1.8 J cm^{-2} which is below the damage threshold (about 2.1 J cm^{-2}) of single pulse irradiation in silica glass.[31] When light intensity is larger than 12 TW cm^{-2}, only type 1 (refractive index increase) with pulse number less than 10 or type 2 modifications with higher pulse number were observed. Both type 1 and type 2 can be used for selective etching,[35] and we can predict that similar polarization-dependent etching enhancement could be observed with type *X* for microfluidic applications.

It is clear that low-loss birefringent modification was observed at both R.R. = 500 kHz and 1 MHz, but the parameter window was larger at 500 kHz for all numerical apertures utilized in our experiments (**Figure 3**a,b) as probably heat accumulation from high energy pulses could prevent the generation of spatially separated nanopores.[36] On the other hand, the retardance is larger at higher repetition rate for low pulse energy. For example, 30 pulses with energy of 550 nJ (7.2 TW cm^{-2}) can imprint type *X* voxels with retardance of 1 nm at 1 MHz, which is 2 times larger than the value of about 0.5 nm at 500 kHz.

To further explore the impact of repetition rate, the evolution of retardance for pulse numbers of 100 and 600, pulse energies of 500 nJ and 1 μJ was investigated. At pulse energy of 1 μJ, only type 2 modification was observed regardless of pulse number and the drop in the retardance with reduced interpulse time ($\lesssim$5 μs) could be attributed to the thermal accumulation (Figure 3c). On the contrary, at pulse energy of 500 nJ, average retardance of voxels was almost unchanged and started to increase for repetition rates higher than 100 kHz for both type *X* (N_p = 100) and type 2 (N_p = 600) modifications (Figure 3d) presumably due to accumulation of defects, e.g., nonbridging oxygen hole centers with

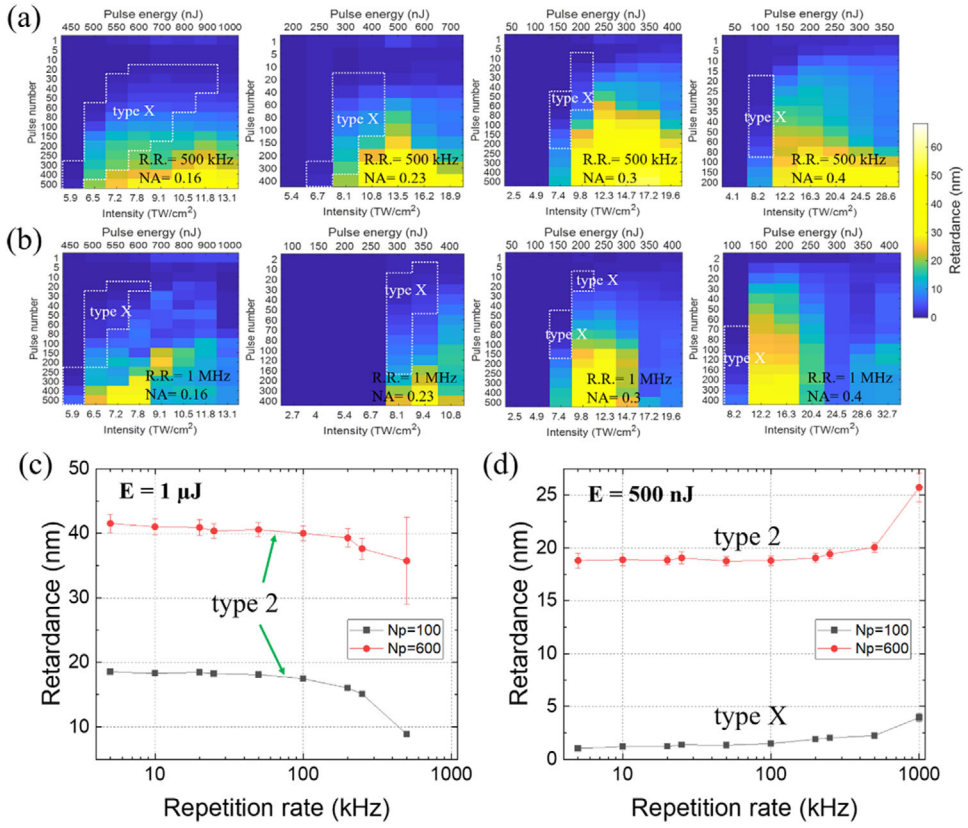

Figure 3. Dependence of retardance on laser parameters with pulse duration of 300 fs. a,b) Retardance maps as functions of pulse energy and pulse number for different numerical apertures (NA = 0.16, 0.23, 0.3, and 0.40) and repetition rates (R.R. = 500 kHz and 1 MHz). The scanning speed for R.R. = 500 kHz and 1 MHz is 1 and 2 mm s^{-1}, respectively. The areas within white dotted lines show the type *X* modification region. c,d) Retardance versus repetition rates for pulse energy 1 μJ and 500 nJ. Each voxel was written by 100 or 600 pulses focused by 0.16 NA lens.

the lifetime (10–20 μs) comparable to the interpulse interval at 100 kHz.[37,38]

The number of retardance and azimuth levels determines the data bits per voxel, which is a crucial factor for high data capacity. The type *X* modification with retardance as high as ≈20 nm at repetition rate of 500 kHz and NA = 0.16 allows multiple retardance levels. To find the limitation of the capacity per voxel, we first analyzed the retardance range and accuracy at pulse energy of 550 nJ with the scanning speed of 1 mm s^{-1} (**Figure 4**a). When the pulse energy was higher than 900 nJ or pulse number larger than 500 for pulse energy from 450 to 800 nJ, only type 2 modification was observed. The ultralow-loss type *X* modification was produced with N_p = 40 to N_p = 300 (Figure 4a,b), which is invisible in an optical image. It is noticeable that the retardance error of type 2 was larger than that of type *X* (Figure 4c) due to larger fluctuations of birefringence produced by variations of aspect ratios of elongated nanostructures. Therefore, the pulse energy of 550 nJ and pulse number from 80 to 300 were used to write birefringent voxels with large retardance range (≈2–20 nm) as well as low azimuth and retardance error (≈0.9° and ≈0.5 nm) (Figure 4d). We managed to demonstrate 7-bit information per voxel with four distinguishable levels of retardance by N_p = 80, 100, 140, and 250 and 32 azimuths at the pulse energy of 550 nJ, and the readout accuracy was nearly 100% (Figure 4e). Although the data capacity is improved by 75% compared with 4 bits per voxel, the drawback is relatively low writing speed of ≈0.2 kB s^{-1}.

Despite 7 bits per voxel was achieved, the large modification size stemming from low NA lens requires relatively large lateral voxel separation of 5 μm, which limits the data capacity. The lens with NA = 0.3 was used to reduce the lateral voxel separation and layer separation to 2 and 17.5 μm, respectively (Figure S4, Supporting Information), and writing of 4 bits per voxel was realized by up to 30 pulses per voxel with R.R. = 1 MHz and scanning speed of 30 mm s^{-1}, leading to ≈9 times higher data capacity and ≈43 times higher recording speed.

For demonstration of ultralow-loss data writing, "The Hitchhiker's Guide to the Galaxy" was written in 100 layers with transmission higher than 99% in the visible range (**Figure 5**). For the data recording, the azimuth was divided into 8 levels and the pulse number of 20 and 30 was used to achieve two distinguishable retardance levels, resulting in 4 bits ($2^3 \times 2^1$) of information per voxel. The data were written from the bottom layer (the 100th layer, 1878 μm beneath the top surface) to the top layer (the first layer, 146 μm beneath the top surface). The text data were encoded by American Standard Code for Information Interchange code, where every two voxels correspond to a character (Figure 5a) and the hexadecimal number of each spot equals Ret. + 2 × Azi. (Ret. = 0, 1; Azi. = 0, 1, ..., 7). The binary retardance and octonary azimuth were normalized and discretized after being extracted

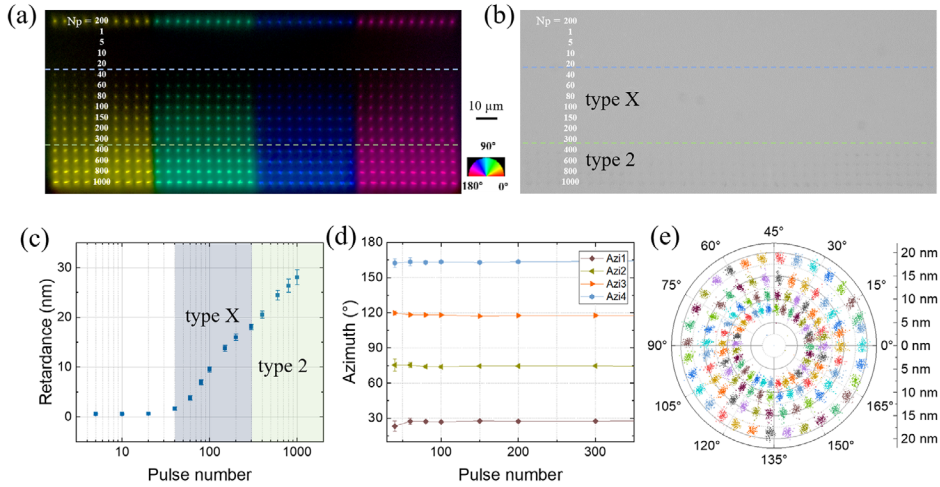

Figure 4. Experimental demonstration of 7 bits per voxel in silica glass. a) The birefringence image of voxels imprinted by four polarizations and different pulse numbers at energy of 550 nJ. b) The optical transmission image of birefringent modifications in (a). c) The retardance dependence on pulse number at pulse energy 550 nJ. The transition from type *X* to type 2 occurs at $N_p = 400$. d) Azimuth for four different slow axes at pulse energy of 550 nJ. e) Polar diagram of the 4 levels retardance and 32 levels azimuth. The 4-level retardance corresponds to N_p =80, 100, 140, and 250. Lateral voxel separation is 5 μm.

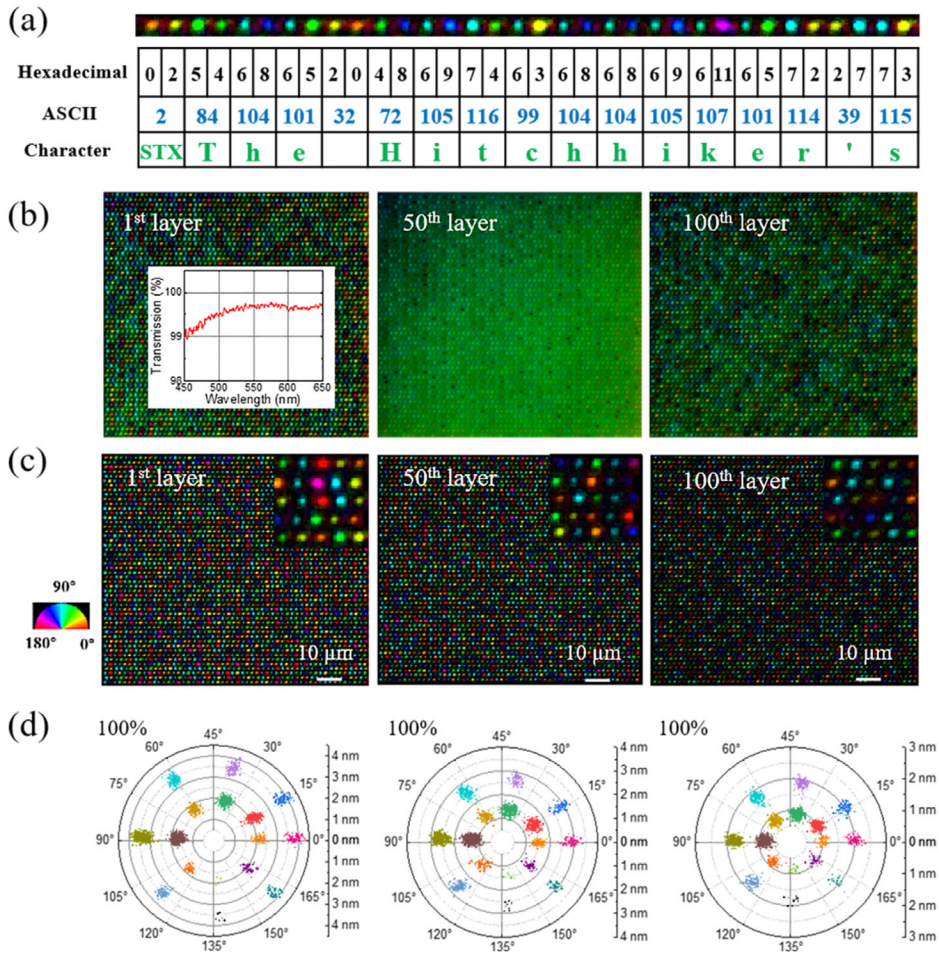

Figure 5. 5D storage of "The Hitchhiker's Guide to the Galaxy." a) Illustration of data encoding and decoding. b) The birefringent images of data voxels of different layers. Inset is the transmission of 100-layer data in the visible range. c) The birefringent images after removing the background of (b). Insets are enlargements of small region (10 μm × 10 μm). d) Polar diagram of the measured retardance and azimuth of all voxels in (c).

from raw data. However, the readout accuracy of recorded data was as low as ≈80%, which can be attributed to the strong background caused by the birefringence of surrounding layers (Figure 5b).

In order to retrieve the data accurately, the strong background was removed by an algorithm to acquire the background-free images with precise retardance and azimuth of each voxel (Figure 5c). The readout accuracy was 100% for all the 1st layer, the 50th layer, and the 100th layer (Figure 5d). The lateral voxel separation and layer separation were decreased to 2 and 17.5 μm, respectively, by using the 0.3 NA lens, corresponding to the data capacity of 350 GB per 127 mm disk and the data writing speed of 8 kB s^{-1} with the scanning speed of 30 mm s^{-1}. The lateral size of voxels increases with writing pulse number. Therefore, the dot separation can be reduced to 1.5 μm using one retardance level produced by 20 pulses, improving the data recording speed to 25 kB s^{-1}. Data recording was demonstrated at 1 MHz, the maximum repetition rate of the Pharos laser. However, type *X* can be observed in preliminary experiment with Satsuma laser operating at repetition rate of 2 MHz, implying data writing speed of 50 kB s^{-1} (Figure S5, Supporting Information).

3. Conclusion

In conclusion, we have demonstrated a 100-layer 5D optical data storage with ultrahigh readout accuracy based on ultralow-loss femtosecond-laser-induced birefringent modification (type *X*) in silica glass. The drop in transmission of single pulse from 100% reveals the start of avalanche ionization. Anisotropic nanopores were produced at a free electron density of 10^{18}–10^{19} cm^{-3} with low writing pulse energy close to the threshold of avalanche ionization, while nanogratings were generated at higher N_e of about 10^{20} cm^{-3}. As the retardance increases with repetition rates at low pulse energy, which is used for type *X* modification, the data writing speed of 8 kB s^{-1} at 1 MHz was achieved for 100-layer 5D data storage of "The Hitchhiker's Guide to the Galaxy" with the retrieved accuracy of 100%. It is possible to achieve the writing speed of ≈400 kB s^{-1} and data capacity of ≈20 TB per disk by reducing pulse number to 10, lateral voxel separation to 0.5 μm, and layer separation to 5 μm with high repetition rate of 10 MHz, but efforts are necessary to reduce the thermal accumulation at high repetition rates.[39]

4. Experimental Section

The writing of birefringent modifications in silica glass was carried out with a mode-locked regenerative amplified femtosecond laser system (PHAROS, Light Conversion Ltd.), operating at a wavelength of 1030 nm with a repetition rate of 5 kHz to 1 MHz and a pulse duration of 190–700 fs. The polarization of the writing laser beam was controlled by a combination of a linear polarizer, an electro-optic modulator, and a quarter waveplate. The laser beam was focused via aspheric lens with different effective NAs (0.16, 0.23, 0.3, and 0.4, Newport) into silica glass sample mounted on a three-axial air-bearing translation stage (Aerotech Ltd.). The writing process was monitored in a real time by capturing the transmitted light passing through the sample with a charge coupled device camera. Laser-induced modifications were produced in the sample with different numbers of laser pulses, pulse energies, and polarization azimuths. The retardance and slow axis orientation of each voxel were quantitatively analyzed with a birefringence measurement system (Cri, Abrio imaging system) integrated into the Olympus BX51 optical microscope operating at 546 nm wavelength. A VIS–NIR microspectrometer CRAIC (integrated into Olympus BX51) was utilized to measure the transmittance of the modified regions. To observe the morphology of nanostructures inside silica glass after laser irradiation, the laser-processed sample was lapped, polished, and etched with a 1 mol L^{-1} KOH solution for 24 h. Imaging of the structures was performed with a SEM (Zeiss Evo50).

Supporting Information

Supporting Information is available from the Wiley Online Library or from the author.

Acknowledgements

The study was supported by the European Research Council (ENIGMA, Grant No. 789116) and Microsoft (Project Silica).

Conflict of Interest

The authors declare no conflict of interest.

Data Availability Statement

The data that support the findings of this study are available from the corresponding author upon reasonable request.

Keywords

nanostructuring, optical data storage, silica glass, ultrafast lasers

Received: October 1, 2021
Revised: December 3, 2021
Published online:

[1] O. Slattery, R. Lu, J. Zheng, F. Byers, X. Tang, *J. Res. Natl. Inst. Stand. Technol.* **2004**, *109*, 517.
[2] M. Irie, Y. Okino, *Jpn. J. Appl. Phys.* **2006**, *45*, 1460.
[3] Z. Sun, J. Zhou, R. Ahuja, *Phys. Rev. Lett.* **2007**, *98*, 055505.
[4] R. R. Gattass, E. Mazur, *Nat. Photonics* **2008**, *2*, 219.
[5] M. Beresna, M. Gecevičius, P. G. Kazansky, *Adv. Opt. Photonics* **2014**, *6*, 293.
[6] A. Papadopoulos, E. Skoulas, A. Mimidis, G. Perrakis, G. Kenanakis, G. D. Tsibidis, E. Stratakis, *Adv. Mater.* **2019**, *31*, 1901123.
[7] B. N. Chichkov, C. Momma, S. Nolte, F. Alvensleben, A. Tünnermann, *Appl. Phys. A: Mater. Sci. Process.* **1996**, *63*, 109.
[8] D. Tan, B. Zhang, J. Qiu, *Laser Photonics Rev.* **2021**, *15*, 2000455.
[9] E. N. Glezer, M. Milosavljevic, L. Huang, R. J. Finlay, T.-H. Her, J. P. Callan, E. Mazur, *Opt. Lett.* **1996**, *21*, 2023.
[10] X. Li, Y. Cao, M. Gu, *Opt. Lett.* **2011**, *36*, 2510.
[11] D. A. Parthenopoulos, P. M. Rentzepis, *Science* **1989**, *245*, 843.
[12] J. F. Heanue, M. C. Bashaw, L. Hesselink, *Science* **1994**, *265*, 749.
[13] H. Ditlbacher, J. R. Krenn, B. Lamprecht, A. Leitner, F. R. Aussenegg, *Opt. Lett.* **2000**, *25*, 563.
[14] P. Zijlstra, J. W. Chon, M. Gu, *Nature* **2009**, *459*, 410.

[15] S. Wu, S. Duan, Z. Lei, W. Su, Z. Zhang, K. Wang, Q. Zhang, *J. Mater. Chem.* **2010**, *20*, 5202.
[16] A. Royon, K. Bourhis, M. Bellec, G. Papon, B. Bousquet, Y. Deshayes, T. Cardinal, L. Canioni, *Adv. Mater.* **2010**, *22*, 5282.
[17] J. D. Mills, P. G. Kazansky, E. Bricchi, J. J. Baumberg, *Appl. Phys. Lett.* **2002**, *81*, 196.
[18] Y. Shimotsuma, P. G. Kazansky, J. Qiu, K. Hirao, *Phys. Rev. Lett.* **2003**, *91*, 247405.
[19] R. Stoian, K. Mishchik, G. Cheng, C. Mauclair, C. D'Amico, J. P. Colombier, M. Zamfirescu, *Opt. Mater. Express* **2013**, *3*, 1755.
[20] Y. Bellouard, A. Champion, B. McMillen, S. Mukherjee, R. R. Thomson, C. Pépin, P. Gillet, Y. Cheng, *Optica* **2016**, *3*, 1285.
[21] Y. Shimotsuma, M. Sakakura, P. G. Kazansky, M. Beresna, J. Qiu, K. Miura, K. Hirao, *Adv. Mater.* **2010**, *22*, 4039.
[22] J. Zhang, M. Gecevicius, M. Beresna, P. G. Kazansky, *Phys. Rev. Lett.* **2014**, *112*, 033901.
[23] R. S. Taylor, C. Hnatovsky, E. Simova, P. P. Rajeev, D. M. Rayner, P. B. Corkum, *Opt. Lett.* **2007**, *32*, 2888.
[24] R. Taylor, C. Hnatovsky, E. Simova, *Laser Photonics Rev.* **2008**, *2*, 26.
[25] F. Zimmermann, A. Plech, S. Richter, A. Tünnermann, S. Nolte, *Opt. Lett.* **2015**, *40*, 2049.
[26] R. Brückner, *J. Non-Cryst. Solids* **1970**, *5*, 123.
[27] R. Drevinskas, P. G. Kazansky, *APL Photonics* **2017**, *2*, 066104.
[28] M. Sakakura, Y. Lei, L. Wang, Y. H. Yu, P. G. Kazansky, *Light: Sci. Appl.* **2020**, *9*, 15.
[29] Y. Wang, M. Cavillon, N. Ollier, B. Poumellec, M. Lancry, *Phys. Status Solidi A* **2021**, *218*, 2100023.
[30] P. P. Rajeev, M. Gertsvolf, P. B. Corkum, D. M. Rayner, *Phys. Rev. Lett.* **2009**, *102*, 083001.
[31] B. C. Stuart, M. D. Feit, A. M. Rubenchik, B. W. Shore, M. D. Perry, *Phys. Rev. Lett.* **1995**, *74*, 2248.
[32] N. M. Bulgakova, V. P. Zhukov, S. V. Sonina, Y. P. Meshcheryakov, *J. Appl. Phys.* **2015**, *118*, 233108.
[33] D. M. Rayner, A. Naumov, P. B. Corkum, *Opt. Express* **2005**, *13*, 3208.
[34] A. Rudenko, J.-P. Colombier, T. E. Itina, R. Stoian, *Adv. Opt. Mater.* **2021**, *9*, 2100973.
[35] E. Casamenti, S. Pollonghini, Y. Bellouard, *Opt. Express* **2021**, *29*, 35054.
[36] M. Lancry, F. Zimmerman, R. Desmarchelier, J. Tian, F. Brisset, S. Nolte, B. Poumellec, *Appl. Phys. B: Lasers Opt.* **2016**, *122*, 66.
[37] C. Corbari, A. Champion, M. Gecevičius, M. Beresna, Y. Bellouard, P. G. Kazansky, *Opt. Express* **2013**, *21*, 3946.
[38] L. Skuja, K. Kajihara, M. Hirano, H. Hosono, *Nucl. Instrum. Methods Phys. Res., Sect. B* **2012**, *286*, 159.
[39] Y. Lei, M. Sakakura, L. Wang, Y. Yu, H. Wang, G. Shayeganrad, P. G. Kazansky, *Optica.* **2021**, *8*, 1365.